Ivashchenko, S.; Escobar Ivirico, JL.; García Cruz, DM.; Campillo Fernández, AJ.; Gallego Ferrer, G.; Monleón Pradas, M. (2015). Bioactive organic inorganic poly(CLMA-co-HEA)/silica nanocomposites. Journal of Biomaterials Applications. 29(8):1096-1108. doi:10.1177/0885328214554816

Bioactive organic–inorganic poly(CLMA-co-HEA)/silica nanocomposites

Sergiy Ivashchenko, Jorge L Escobar Ivirico, Dunia M García Cruz, Alberto Campillo-Fernández, Gloria Gallego Ferrer and Manuel Monleón Pradas

J Biomater Appl published online 6 October 2014
DOI: 10.1177/0885328214554816

JOURNAL OF
biomaterials applications

Journal of Biomaterials Applications
0(0) 1–13

DOI: 10.1177/0885328214554816
jba.sagepub.com
SAGE

Bioactive organic–inorganic poly(CLMA-co-HEA)/silica nanocomposites

Sergiy Ivashchenko[1], Jorge L Escobar Ivirico[1], Dunia M García Cruz[1], Alberto Campillo-Fernández[2], Gloria Gallego Ferrer[1,3] and Manuel Monleón Pradas[1,3]

Abstract

A series of novel poly(CLMA-co-HEA)/silica nanocomposites is synthesized from caprolactone 2-(methacryloyloxy)ethyl ester (CLMA) and 2-hydroxyethyl acrylate (HEA) as organic comonomers and the simultaneous sol-gel polymerization of tetraethyloxysilane (TEOS) as silica precursor, in different mass ratios up to a 30 wt% of silica. The nanocomposites are characterized as to their mechanical and thermal properties, water sorption, bioactivity and biocompatibility, reflecting the effect on the organic matrix provided by the silica network formation. The nanocomposites nucleate the growth of hydroxyapatite (HAp) on their surfaces when immersed in the simulated body fluid of the composition used in this work. Proliferation of the MC3T3 osteoblast-like cells on the materials was assessed with the MTS assay showing their biocompatibility. Immunocytochemistry reveals osteocalcin and type I collagen production, indicating that osteoblast differentiation was promoted by the materials, and calcium deposition was confirmed by von Kossa staining. The results indicate that these poly(CLMA-co-HEA)/silica nanocomposites could be a promising biomaterial for bone tissue engineering.

Keywords

Nanocomposites, organic polymer, silica, bioactivity, biocompatibility

Introduction

Copolymer networks of caprolactone 2-(methacryloyloxy)ethyl ester (CLMA) and 2-hydroxyethyl acrylate (HEA) have demonstrated excellent potential as substrates for tissue engineering.[1,2] The main component, PCLMA, has a polycaprolactone side-chain, which can be cleaved hydrolytically, thus making PCLMA a semi-degradable material, a property that can be of interest in applications. Moreover, its monomer CLMA can be easily copolymerized with other co-monomers as a way to tailor the hydrophilicity of the resulting material; the addition of different amounts of the hydrophilic monomer HEA to the hydrophobic CLMA leads to copolymers with modulated water uptake in wet environments.[3] The HEA co-monomer improves the toughness of PCLMA and facilitates the diffusion of water and nutrients across the material.[1,3] An adequate hydrophobic/hydrophilic balance in synthetic materials is fundamental for cell adhesion, proliferation, differentiation and extracellular matrix production, which depend strongly on the hydrophilicity of the substrate.[4,5] In general, high hydrophilic character reduces cell adhesion on the substrate and intermediate hydrophilicity promotes it.[5] Our previous works demonstrated that P(CLMA-co-HEA) networks with intermediate hydrophilicity (with around a 30 wt% of HEA) are the best candidates in this system for the culture of bone marrow stromal cells[2] and human chondrocytes[5] in terms of cell adhesion, proliferation and differentiation.

[1]Center for Biomaterials and Tissue Engineering, Universitat Politècnica de València, Valencia, Spain
[2]Applied Thermodynamics Department, Universitat Politècnica de València, Valencia, Spain
[3]Networking Research Center on Bioengineering, Biomaterials and Nanomedicine, (CIBER-BBN), Valencia, Spain

Corresponding author:
Sergiy Ivashchenko, Center for Biomaterials and Tissue Engineering, Universitat Politècnica de València, 46022 Valencia, Spain.
Email: seriv@posgrado.upv.es

When thinking about these materials for bone tissue engineering (TE), besides cell response, other important requirements such as mechanical strength and bioactivity must be considered.[6–8] The mechanical properties of pure homopolymers of interest in bone TE are usually not high enough to withstand the loads when implanted and require reinforcement. A common strategy for this purpose is their combination with inorganic particles of, for instance, bioglass, hydroxyapatite and tricalcium phosphate.[9–19] Commonly, these fillers are incorporated into the matrix polymer through dispersion into a polymer solution. Most of the time, the solution viscosity, the nature of the interface and the later processing of the mixture cause particle agglomeration and a defective interfacial bonding, leading to a poor reinforcement. The hybridation of the organic matrix with a silica network obtained by the simultaneous joint polymerization of the organic phase and a silica precursor, such as tetraethyl orthosilicate (TEOS), has been presented as a better strategy for mechanical reinforcement.[20–26] The silica network not only improves the mechanical properties of the organic matrix, but also provides the system with a greater bioactivity,[27–29] which is required for the successful osseointegration of the biomaterial. Bioactivity refers to the ability of materials to induce an apatite-like interface between the biomaterial and bone host tissue.[24,27,30,31] The increased bioactivity of these nanocomposites is a consequence of the dissolution of silica in biological fluid leading to the formation of negatively charged ≡Si-OH groups able to act as nucleation sites for the calcium ions of apatite.[30,32]

Silica-based organic–inorganic nanocomposites obtained by the polymerization of the organic phase during the simultaneous *in situ* sol-gel polymerization of silica precursors possess morphological characteristics that strongly influence their properties.[21,24,30] Previous works on these systems concluded the inorganic network can be homogeneously interdispersed or interpenetrated with the organic matrix. Furthermore, for silica contents below the percolation threshold, which in our case was around 15%, the inorganic phase is uniformly dispersed as nanoporous nanoparticles with aggregates defining pores of tens of nanometres. These aggregates are isolated in the organic matrix and preserve the nanometric nature with dimensions below 400 nm. For silica contents above that threshold, the silica network becomes continuous through the sample and totally interpenetrates with the organic phase; both phases, the organic and the inorganic ones, are then co-continuous. The formation of a continuous inorganic phase marks a change in material's behaviour and has a high impact on its strength, chain mobility, water sorption and bioactivity.[33–36]

The present work studies how the silica network affects chemical and mechanical properties of the nanocomposites, of special interest in bone TE, such as the water contact angle, equilibrium water sorption, mechanical strength, bioactivity and pre-osteoblast proliferation and differentiation.

Material and methods

Chemicals

Caprolactone 2-(methacryloyloxy)ethyl ester (CLMA) (Sigma-Aldrich, Spain) and 2-hydroxyethyl acrylate (HEA) (Sigma-Aldrich, Spain, 96% pure) were employed as co-monomers without further purification. Benzoyl peroxide (BPO) (Sigma-Aldrich, Spain, 97% pure) and ethylene glycol dimethacrylate (EGDMA) (Sigma-Aldrich, Spain, 99% pure) were used as initiator and crosslinker, respectively. Tetrahydrofuran (THF) (Sigma-Aldrich, Spain, 99% pure), ethanol (Sigma-Aldrich, Spain, 99.5% pure), n-octane (Sigma-Aldrich, Spain, 98% pure) and extra pure distilled water of 10 μS/m conductivity (Scharlau, Spain) were used as solvents. Tetraethoxysilane (TEOS) (Sigma-Aldrich, Spain, 99% pure) was used as silica precursor, and hydrochloride acid (HCl) (Scharlau, Spain, 37%) as catalyst of the silica formation reaction.

Synthesis of poly(CLMA-co-HEA)/silica nanocomposites

Nanocomposites were obtained in a simultaneous polymerization of the organic and the inorganic precursors, with different mass ratios of both components, as described in previous work.[20,33,35] Briefly, the organic network precursors were prepared by mixing the CLMA and HEA monomers in a 60:40 mass ratio with a 0.1 wt% of EDGMA, 1 wt% of BPO, and 13 wt% of THF. The quantity of inorganic silica precursor (TEOS) required to achieve nanocomposites with a final silica content of 0, 5, 10, 15, 20, 25 and 30 wt% was determined assuming total conversion of the sol-gel reaction, and was mixed with distilled water and HCl in a molar ratio TEOS: H_2O: HCl = 1:2:0.0185. After 30 min of stirring, the solutions of the organic and the inorganic precursors were mixed and stirred for another 30 min. Then, they were poured into moulds consisting in two glass plates with a nylon cable in between, in order to obtain 1 mm thick films, and were polymerized at 60°C for 24 h. The resulting films were washed in a boiling mixture of ethanol/water (30/70 v/v, with boiling point at ≈87°C) for 24 h and then dried in vacuum to constant weight. The materials were kept in a sealed jar with silica gel to prevent ambient water absorption.

Thermogravimetric analysis (TGA)

Thermal degradation profiles were obtained with a SDT-Q600 thermogravimeter (TA-Instruments, USA). Copolymer and nanocomposite samples (5–10 mg of weight) were placed on the balance and heated from 50 to 700°C at a rate of 10°C/min.

Density measurements

The densities of all materials were determined according to the formula

$$\rho_{\text{sample}} = \frac{m_{\text{air}}}{m_{\text{air}} - m_{\text{solvent}}} \cdot \rho_{\text{solvent}} \quad (1)$$

where m_{air} and m_{solvent} signify the weights of the sample in air and immersed in n-octane, respectively, and ρ_{sample} and ρ_{solvent} represent the densities of the sample and n-octane, respectively. n-Octane was chosen for not being a solvent and having a lower density than the materials. A Mettler Toledo AX205 balance accessory was used for weighing the samples. The specific volume (v) was calculated as the inverse of density. Six replicas per composition were used for the experiments.

Differential scanning calorimetry (DSC)

DSC scans of all samples were obtained in a DSC 823E apparatus (Mettler Toledo, Spain). After erasing the effects of any previous thermal history, samples of 5–7 mg weight were subjected to a cooling scan down to −90°C at 40°C/min, followed by a heating scan until 120°C at 10°C/min. The glass transition temperature, T_g, was obtained as the temperature of the inflexion point of the heating scan curve for each composition; the width of the glass transition, ΔT_g, was determined as the temperature difference between the onset and endpoint of the glass transition. The specific heat capacity jump at the glass transition per gram of nanocomposite, Δc_p, was determined as the difference of c_p between endpoint and onset of the glass transition. The ratio between the number of polymer units undergoing the glass transition in the nanocomposites and in the neat copolymer, x, was calculated as

$$x = \frac{\Delta c_{p\ \text{nanocomp}}}{\omega \cdot \Delta c_{p\ \text{copol}}} \quad (2)$$

where ω is the actual mass fraction of the copolymer in the composite.

Dynamic mechanical analysis

Dynamic mechanical analysis (DMA) of dry samples (bars of rectangular cross section ca. $10 \times 4.5 \times 1\,\text{mm}^3$) was performed in a Seiko DMS210 apparatus (Seiko Instruments Inc., Japan) at a frequency of 1 Hz in the tension mode. The temperature dependence of the storage modulus and loss tangent was measured in the temperature range from −75°C to 150°C at 2°C/min.

Water uptake measurements

The water uptake was determined gravimetrically using a Mettler Toledo AX205 balance accessory. Dry disks (8 mm diameter and 1.0 mm thickness) were cut from the polymerized plates. Swelling experiments were performed by immersing the dry disks in distilled water at 37.0 ± 0.1°C until equilibrium. The equilibrium water content (EWC) was expressed as the amount of water absorbed by the sample per unit mass of the dry polymer

$$EWC = \frac{m_{\text{water}}}{m_{\text{dry\_disks}}} \quad (3)$$

Equilibrium was attained in around 48 h. Measurements were repeated five times for each composition.

Contact angle measurements

In order to determine the wettability of the samples' surface, contact angle measurements were conducted in air atmosphere with the sessile drop method, employing water (extra pure, Scharlau, Barcelona, Spain) as liquid. A OCA20 instrument (DataPhysics Instruments GmbH, Germany) was used for this purpose. A 1 mL syringe was employed as dropper. A minimum of five drops per sample was analysed.

Bioactivity assay

A simulated body fluid (SBF) free of proteins with ion concentration, pH and temperature nearly equal to human blood plasma was employed as medium for *in vitro* assessing the bioactivity of the materials.[16,27] Disks of the neat copolymer and nanocomposites (with 15 and 30 wt% content of silica) were vertically suspended by a cotton thread in closed glass vials filled with SBF at 37°C. The ratio of the sample's surface area to the volume of solution was $12\,\text{mm}^2\,\text{ml}^{-1}$, slightly higher than the Kokubo and Takadama proposal.[31,37] The SBF solution was not renewed during the first seven days; afterwards, a solution with twice the ion concentrations of SBF was employed which was renewed each 2–3 days to provide more favourable conditions for apatite growth.[32] Samples were withdrawn from the SBF after 7, 14 and 21 days, gently washed with ultra-pure water and dried in vacuum at 40°C.

The morphology of nucleated apatite on the samples was observed using a JEOL JSM-5410 (JEOL Ltd., Japan) scanning electron microscope, SEM, at a 20 kV acceleration voltage and 15 mm of working distance, and the samples were sputter-coated with gold. The chemical composition of the nucleated apatite was determined by means of an Energy Dispersion Spectrometer, EDS (Oxford Instruments, UK), connected to the SEM. Calcium/phosphorous atomic ratios were calculated dividing the atomic percentages of these elements proportioned by EDS. The element spectra were taken on carbon-coated samples at a 10 kV acceleration voltage and 15 mm of working distance. Copper was used as optimization standard.

Cell proliferation and differentiation assay

The immature osteoblast-like MC3T3-E1 cell sub-line (RIKEN Cell Bank, Japan) from passage 12 was seeded on disks of the copolymer and the nanocomposites with 5, 15 and 30 wt% of silica content, previously sterilized by gamma radiation (25 kGy) and pre-conditioned with culture medium without FBS, at a cellular density of 5×10^3 cells/disk. After 1 hour of incubation for cell adhesion at 37°C with 5% CO_2, 400 µl of fresh medium (DMEM supplemented with 10% of FBS and 1% of penicillin/streptomycin solution) was added to each well and renewed every three days. Samples were incubated for 1, 7, 14 and 28 days at 37°C with 5% CO_2. Thermo Scientific Nunc™ Thermanox polystyrene coverslips (Thermo-Fisher Scientific, Spain) were used as control substrates.

Cell proliferation was assessed by the MTS assay using CellTiter 96® AQueous One Solution Cell Proliferation Assay Kit (Promega, Spain), and spectrophotometer Victor 1420 Multilabel Counter (PerkinElmer, Spain). Cell proliferation was quantified from the optical density (OD), using a calibration curve that converted the OD into number of MC3T3-E1 cells.

Osteoblastic differentiation was evaluated after 14 days of culture by immunocytochemistry. Samples were washed with 0.1 M of PBS, fixed for 1 hour with 4% paraformaldehyde and incubated for 2 h at room temperature with a blockade solution (BS) (8.9 mL of PBS (0.1 M), 1 mL of FBS (10%) and 0.1 mL of Triton x-100 (0.1%)). Afterwards, samples were incubated with the mixture of antihuman rabbit collagen I antibody (Chemicon, Temecula, CA, USA) (for type I collagen) and antihuman mouse osteocalcin antibody (R&D Systems, USA) (for osteocalcin detection) in blockade solution for 1 h at room temperature (RT) and overnight at 4°C. Then, the samples were washed three times with PBS (0.1 M) and incubated for 2 h at RT in dark with the secondary fluorochrome-conjugated antibodies (1:200 in blockade solution) goat anti-rabbit Alexa Fluor 647 and goat anti-mouse Alexa Fluor 488 (Jackson Immunoresearch, West Grove, PA, USA). Subsequently, samples were washed three times with PBS 0.1 M at RT and prepared with Vectashield Mounting Medium with DAPI (Vector Laboratories, Burlingame, CA, USA). Finally, a Leica TCS SP2 AOBS (Leica Microsystems Heidelberg GmbH, Germany) confocal laser-scanning microscope (CLSM) was used to observe the samples. Two-dimensional pseudocolour images (255 colour levels) were recorded with a size of 1024 × 1024 pixels.

Von Kossa staining

Samples after 14 and 21 days of culture fixed with paraformaldehyde as described in 2.10 were washed two times with DPBS and then incubated in 5% $AgNO_3$ solution in demineralized water for 30 min under mild UV exposure. Afterwards, samples were washed two times with distilled water to eliminate all precipitated solution, counterstained with 1% neutral red acidified solution for 2 min, washed one more time with distilled water and observed under light microscope.

Statistical analysis

Data were expressed as mean ± standard deviation (SD). A one-way ANOVA test was used to conduct statistical analysis, and statistical significance was accepted at the probability level $P < 0.05$.

Results

Synthesis and characterization of the poly(CLMA-co-HEA)/silica nanocomposites

Poly(CLMA-co-HEA)/silica nanocomposites with silica contents up to a 30 wt% were successfully obtained as homogeneous transparent plates of 1 mm of thickness, with notable increase of their hardness and brittleness with an increasing silica content. An adequate reaction was confirmed by infrared spectra of the materials (Figure 1) that showed the band between 3500 and 3200 cm^{-1} of the hydroxy groups (−OH) and the band at 1700 cm^{-1} of the C = O groups present in both monomers (CLMA and HEA), which decreased with the silica content. Silica fingerprint appeared as small peaks at 1080–1024 and 800 cm^{-1}, attributed to the Si-O-Si asymmetric and symmetric stretching vibration, respectively.

The specific volumes of nanocomposites decreases steadily with the silica content (Figure 2a) and lie, approximately, on the straight line joining the values of the pure copolymer and pure silica glass obtained by curing at 900°C.[38] The thermal degradation curves of

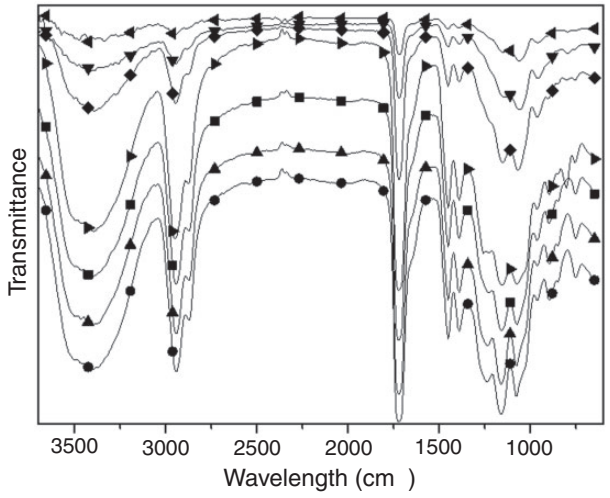

Figure 1. FTIR spectra of the materials: 0 (●), 5 (▲), 10 (■), 15 (►), 20 (♦), 25 (▼) and 30 (◄) wt% of silica.

the materials (TGA) show no solid residue for the copolymer, but increasing amounts for the nanocomposites. These residues at 650°C allowed determining the actual amount of silica in the nanocomposite samples (Table 1, Figure 2b).

The DSC thermograms of all the compositions are shown in Figure 3(a). No crystallization or melting processes were detected. The copolymer shows a single glass transition, with a mid-point T_g around −19.0°C, and in the nanocomposites, T_g increases steadily with the silica content (Figure 3b).

The dynamic-mechanical temperature scan at 1 Hz of the copolymer shows the main relaxation process associated to the glass transition as a sharp drop of the storage modulus (E') between −25°C and 50°C (Figure 4a). In the corresponding loss tangent thermogram, a shoulder appears on a main peak corresponding to the relaxation, which could be indicative of a certain degree of phase separation or heterogeneity in

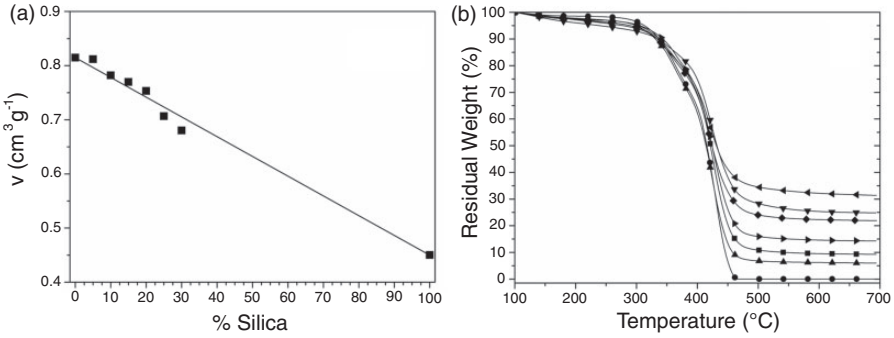

Figure 2. (a) Specific volume of the materials as a function of the silica mass percentage. A value of 0.455 cm^3/g has been taken for pure silica glass (100% silica).[38] (b) Residual weight as a function of temperature determined by TGA for all the materials: 0 (●), 5 (▲), 10 (■), 15 (►), 20 (♦), 25 (▼) and 30 (◄) wt% of silica.

Table 1. Characteristica of the nanocomposites bare and coated by hydroxyapatite.

Expected silica content (%wt)	Actual silica content (%wt)	EWC (%)	θ (°)	Ca:P ratio	
				14d	21d
0	0	28.8 ± 1.4	93.3 ± 2.6	1.7 ± 0.1	1.9 ± 0.1
5	5.6 ± 2.9	28.9 ± 1.1	94.7 ± 0.3	–	–
10	9.5 ± 2.1	29.4 ± 1.0	85.1 ± 1.5	–	–
15	16.3 ± 2.1	29.0 ± 1.0	78.6 ± 2.2	1.6 ± 0.1	1.8 ± 0.2
20	20.4 ± 3.2	28.5 ± 1.5	77.6 ± 1.7	–	–
25	28.2 ± 3.6	25.4 ± 1.7	71.3 ± 1.0	–	–
30	33.3 ± 2.7	16.0 ± 0.8	76.8 ± 0.7	1.6 ± 0.1	1.9 ± 0.2

Note: Expected silica content (from the reactant formulation) and actual silica content (from the weights of the TGA residues) of the bare materials, equilibrium water content EWC and water contact angle θ of the bare materials, Ca:P atomic ratio of the hydroxyapatite grown on the materials' surfaces after 14 and 21 days, as calculated from the EDS signal intensities.

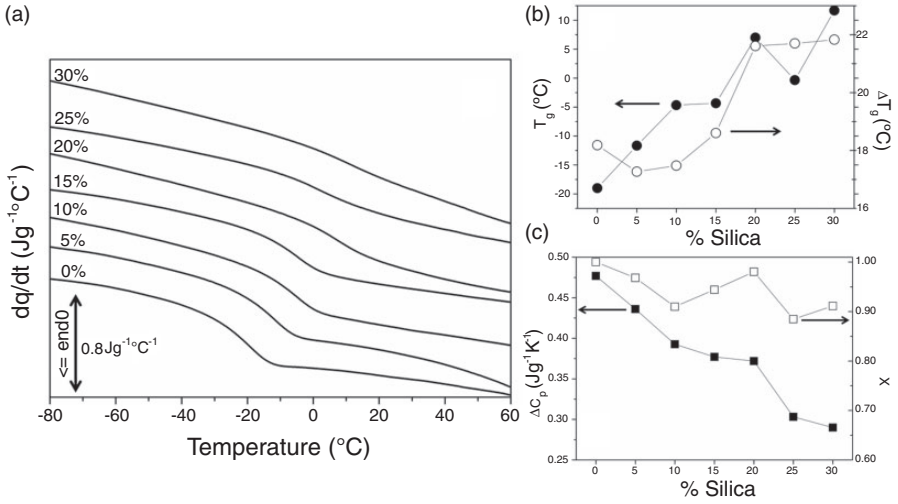

Figure 3. (a) Normalized heat flow on heating for neat copolymer and nanocomposites as a function of temperature; (b) dependence of Tg, ΔTg and (c) Δcp and x with the silica content in the materials.

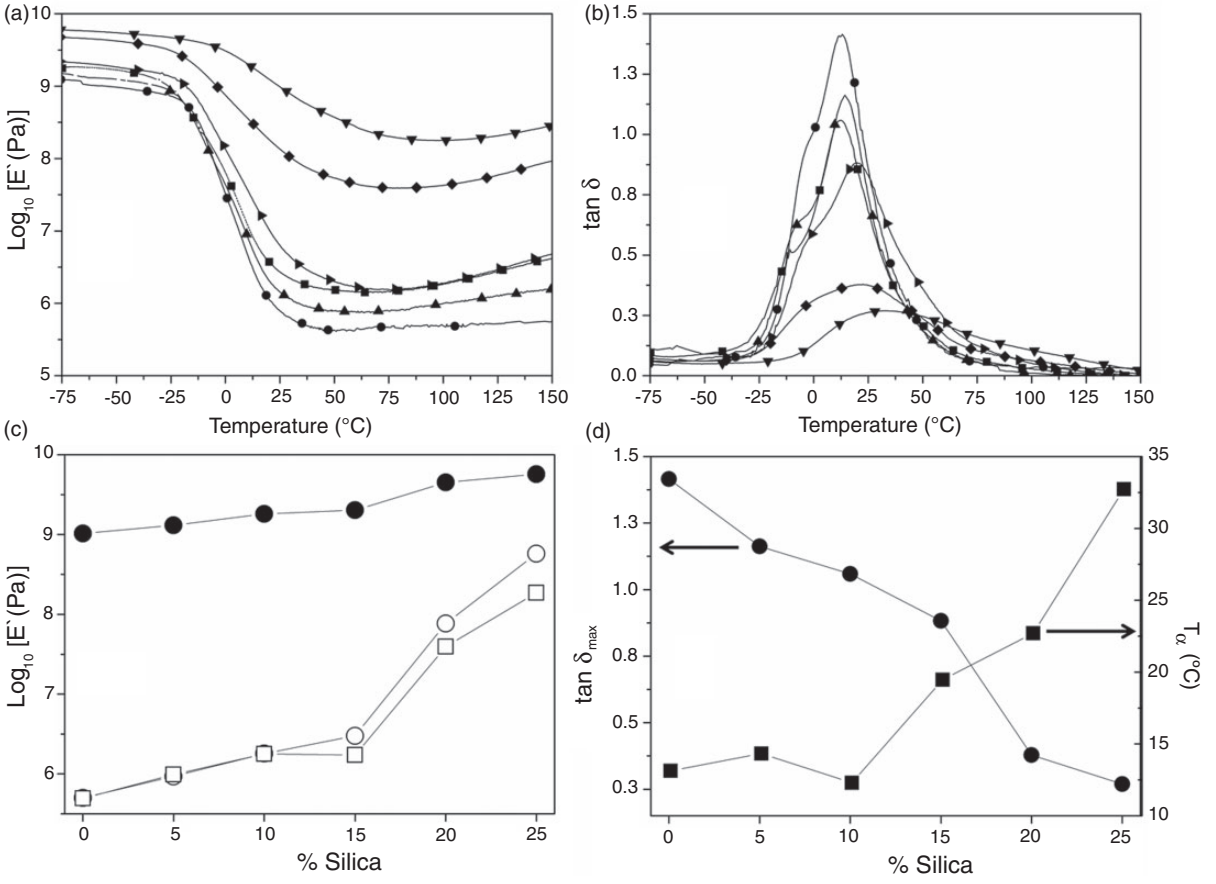

Figure 4. Logarithm of the storage modulus (a) and the loss tangent (b) as a function of temperature for the materials: 0 (●), 5 (▲), 10 (■), 15 (►), 20 (♦), and 25 (▼) wt% of silica. Dependence of storage moduli on silica content in the glassy (●, T = −60°C) and rubbery (□, T = 100°C) states, as well as at body temperature (○, T = 37°C). (c) Maximum values of loss tangent at the relaxation peaks and their temperatures. (d) The 30 wt% silica sample could not be measured due to its brittle nature.

the copolymer (Figure 4b), which was non-detectable by DSC.

Bioactivity

The SEM images (Figure 5a) show the nucleated hydroxyapatite (HAp) on the samples' surfaces after 7, 14 and 21 days of incubation in SBF. EDS spectra show that this coating is mainly composed of calcium and phosphorous, with a Ca/P atomic ratio close to the stoichiometric one of apatite, 1.67, especially for the 15% SiO_2 samples (Table 1, Figure 5b). After 7 days of incubation in SBF, few hydroxyapatite nuclei grew on the material's surface, showing better coating on the 30% silica sample. After 14 and 21 days of incubation, the neat copolymer and the 15% silica samples were completely coated with 2–3 layers of the typical porous HAp cauliflowers formed by needle-shaped crystals, while the 30% silica samples coating had some imperfections.

Cell proliferation and differentiation

The results of the MTS assay for the MC3T3-E1 cells seeded on the samples with 0, 5, 15 and 30 wt% of SiO_2. The number of viable cells on the materials was always of the same order as the positive control at culture days 1 and 7, but it was significantly greater than the positive control at day 21, the greater the larger the silica content of the sample (Figure 6).

As seen by confocal laser scanning microscopy (Figure 7), the MC3T3-E1 osteoblast-like cells expressed type I collagen as well as osteocalcin, both characteristic markers of osteoblastic differentiation and of the beginning of osteogenesis. Cells with fibroblast-like appearance were not observed on all samples. Cells grown on the neat copolymer showed predominantly cuboidal appearance and lesser expanded morphology, while those cultivated on the nanocomposites had a more elongated shape, showing the development of cellular processes.

The images of von Kossa staining taken with light microscope detected abundant calcium deposition for 14 (Figure 8a) and 21 (Figure 8b) days of culture. In this type of staining, silver ions replace calcium in phosphates and carbonates, and then are reduced under UV to black metallic silver, allowing to visualize indirectly the presence and distribution of calcium deposits as black spots.

Discussion

The close match between the nominal and the actual silica contents of the nanocomposite materials (Table 1) indicate that the simultaneous sol-gel polymerization of both networks proceeds with a high degree of conversion. Discrepancies between both values are attributable to incomplete polymerization of organic phase and subsequent partial elimination of low molecular weight chains during washing. The materials were optically transparent and progressively more rigid as the percentage of silica increased. By analogy with similar silica nanocomposites,[36] optical transparency of all composites confirmed that the silica particle aggregates were very small and did not exceed 400 nm size.

The linear decrease of the specific volume of the nanocomposites with increasing silica content suggests there is no excess volume, that is, the molecular free volume of both the inorganic and organic phases is the same in the composites as it is in the neat copolymer and in pure silica.[38] Since the polymerization of silica is faster than that of the organic polymer, this fact implies that the organic chains are efficiently filling the pores left by the silica structure and intimately interpenetrate with the particles without voids or vacancies. The same efficient filling of the silica network pores by the polymer phase was observed by Rodríguez et al. in PHEA/silica nanocomposites,[33] and by Vallés et al. in poly(EMA-co-HEA)/silica nanocomposites,[36] both synthesized by a similar procedure, also explained by the polymerization of silica taking place before the polymerization of the organic phase.[33,35]

These nanocomposite systems have a definite structure build-up that is reflected in their properties. Studies on other polymer-silica nanocomposites[33,35,36] showed that for silica contents below a percolation threshold (10–15% for PHEA/SiO_2 nanocomposites,[33] and $\approx$15% for poly(EMA-co-HEA)/SiO_2 nanocomposites[35,36]), the silica network is in the form of inorganic aggregates that are isolated in the organic matrix; as the silica content is raised above a percolation threshold, both phases become co-continuous, and greater silica contents result in a finely interpenetrated silica phase with the polymer matrix. Traces of this structural transition can be discovered in the composition-dependence of the different physical properties of the materials. The steady increase of T_g silica content is a consequence of the restriction of the molecular mobility of the organic polymer due to its interpenetration with the much more immobile silica network chains. The width of the glass transition (ΔT_g) is a measure of the heterogeneity of the polymer domains undergoing glass transition; a narrow glass transition is indicative of the homogeneity of the cooperatively rearranging molecular regions that relax during the transition, while large ΔT_g values are indicative of the heterogeneity of those domains. In our materials, ΔT_g is, for silica contents below 15%, similar in the nanocomposites and in the neat copolymer; it sharply increases at around 15%, and the more silica-rich samples have much wider glass transition

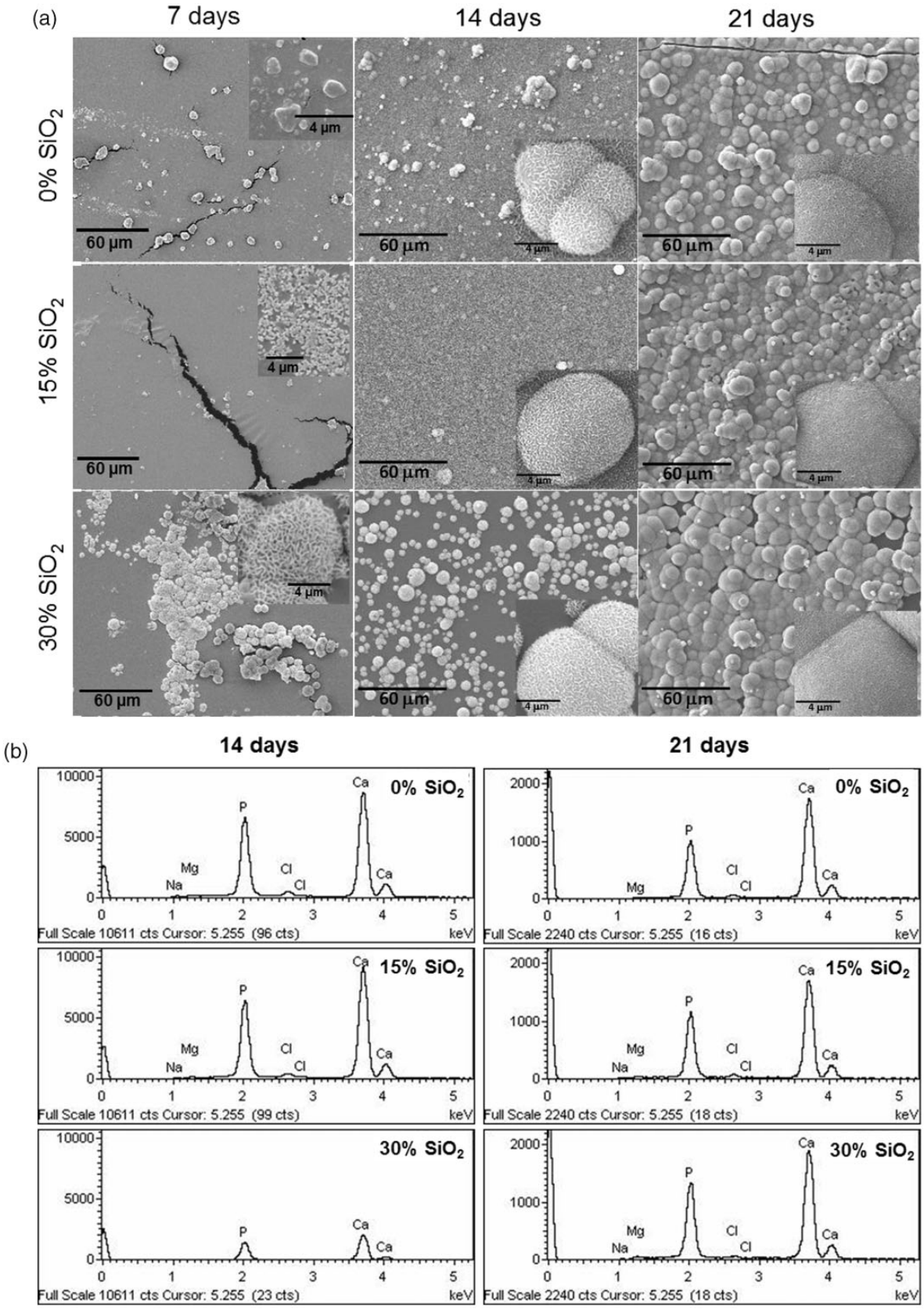

Figure 5. (a) SEM images and (b) EDS spectra of hydroxyapatite nucleated on the surface of the on samples with 0, 15 and 30 wt% of silica content after 7, 14 and 21 days of immersion in SBF.

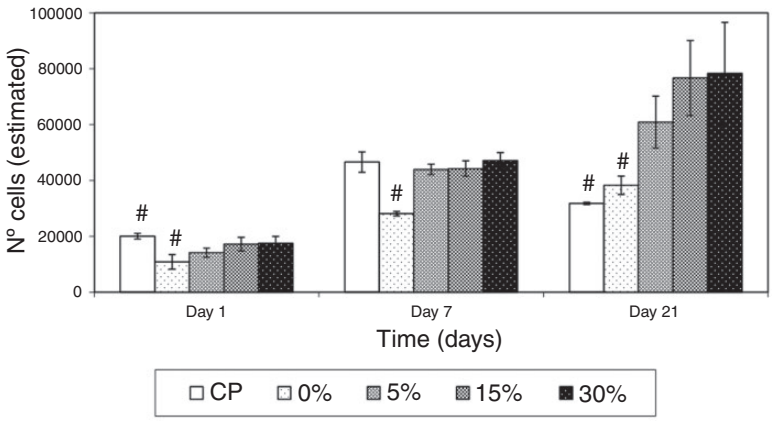

Figure 6. Viable cells (MTS assay) on samples with 0, 5, 15 and 30 wt% of silica content for 1, 7 and 21 days of culture. # denotes significant differences among samples for the same culture time ($P < 0.05$).

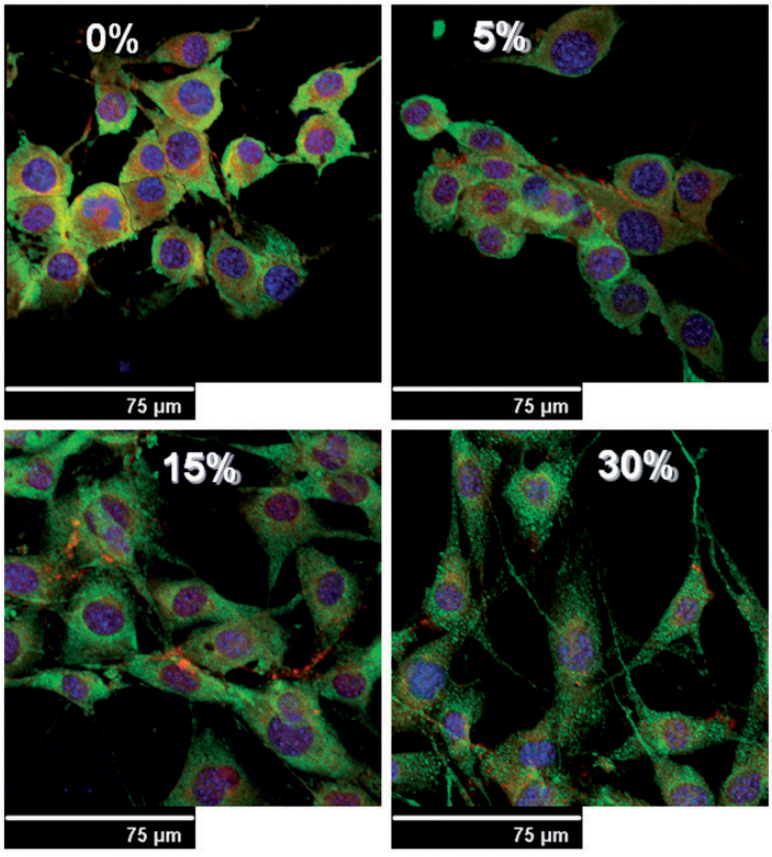

Figure 7. MC3T3-E1 osteoblast-like cell line cultured for 14 days on the copolymer and nanocomposites, seen through CLSM for markers of cell nuclei (DAPI, blue), collagen I (red), and osteocalcin (green).

(Figure 3b). The change in the topology of the silica domains from a disconnected phase to a continuously interpenetrated phase is thus reflected on the relaxation of the organic polymer chains across their glass transition. The heat capacity jump at T_g for a polymer, Δc_p, is proportional to the number of units whose degrees of freedom were frozen below T_g and become mobile above it. In our neat copolymer, Δc_p is $0.48\,Jg^{-1}K^{-1}$ and this quantity decreases steadily with increasing silica content in the nanocomposite series (Figure 3c), telling that a decreasing number of polymer chains in the nanocomposites is undergoing conformational

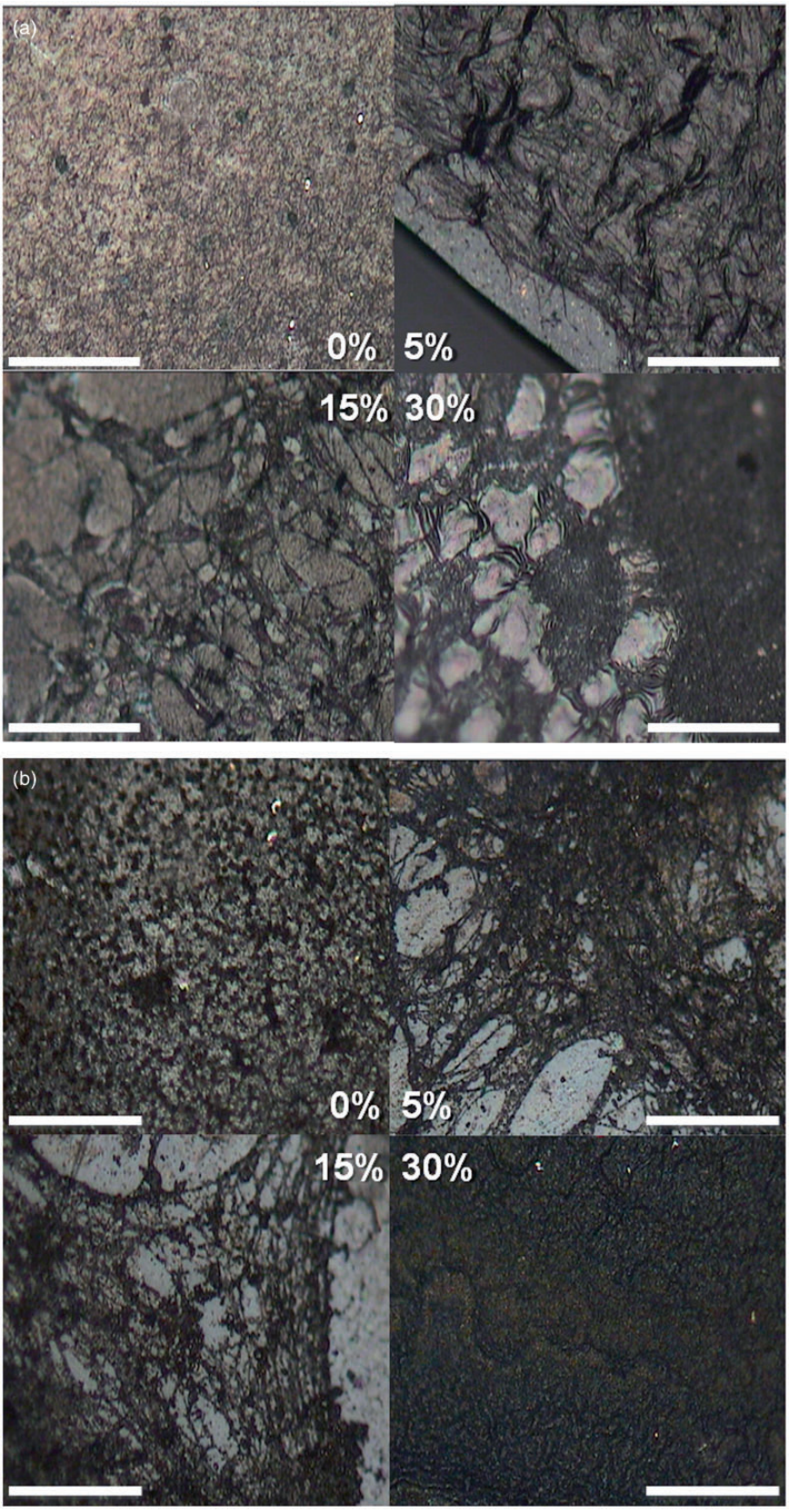

Figure 8. Light microscope images of von Kossa staining of MC3T3-E1 osteoblast-like cell line cultured for 14 (a) and 21 (b) days on the copolymer and nanocomposites. Scale bar, 100 μm.

motions during the glass transition. The quantity × swiftly falls from unity for the neat copolymer to around 0.9 for the 30% silica sample (Figure 3c), indicating that the interpenetration with the silica network not only alters the local environment of the relaxing units (as ascertained by the broadening of ΔT_g), but also does impede the motions of a (small) fraction of the organic chains at T_g.

The effect of the silica phase on the mechanical properties of the nanocomposites is to increase, as expected, the mechanical modulus both in the glassy and in the rubbery state. In this latter state, the transition from the disconnected to the continuous topology of the silica phase is clearly reflected as a marked modulus increase from the percolation silica content onwards (Figure 4c). The damping properties of the materials, as reflected in the loss angle δ, follow an expected trend, decreasing with increasing silica content of the nanocomposites (Figure 4d), while slightly shifting towards higher temperatures (Figure 4d), due to the altered conditions of the organic chain mobility caused by the organic–inorganic polymer interaction, consistently with the DSC results. The nanocomposites have Young moduli that range, at body temperature, from under 1 MPa to over 100 MPa: almost a three-order magnitude interval, which permits to tailor this property to the mechanical needs of intended applications for bone-tissue engineering.

The nanocomposite series is as hydrophilic as the neat copolymer up to around the 20% silica mass percentage sample, as revealed by the equilibrium water content (Table 1). The EWC value then drops to a minimum of 16% for the 30% silica sample. These results can, again, be explained by the formation of the silica network: below the percolation threshold, silica phase does not significantly restrict the swelling of the organic matrix, and free silanol groups on its phase boundaries counterbalance the loss of hydrophilicity due to this constraint. When the silica network becomes continuous, the swelling of the organic network is greatly reduced; moreover, there are less boundary silanol groups, since the silica domains have merged into a single network. The water contact angle is a property sensitive to the presence of these surface silanol groups (Table 1). At the lowest silica content, the contact angle is similar to that of the neat copolymer, then drops as a consequence of increasing polarity of the material's surface due to the free silanols, and finally increases in the 30% sample, in which a densely continuous silica network has less boundary silanols. This result is of great importance, as surface properties play a significant role in the material's bioactivity and in cell adhesion onto it.

The apatite nucleation ability of the copolymer's surface can be explained by presence of polar groups (carboxy and hydroxy) that interact electrostatically with Ca^{2+} ions from the SBF, forming nucleating sites that attract phosphate ions resulting in calcium phosphate coating. Besides these same polar groups, the nanocomposite possess also silanol groups that may start the nucleation process of hydroxyapatite. According to previous works,[27,30] the nature of the first HAp layer and the kinetic of its formation in nanocomposites essentially depends on the silica content and the connected or disconnected topology of silica phase. The HAp growth on the hybrid-SBF interface is promoted by the dissolution of the existent silica network, which produces a large number of non-condensed terminal silanols that serve as nucleation sites.[27,32] A maximum apatite growth was observed in our materials below silica percolation concentration ($\leq$15 wt% of silica), while the 30 wt% nanocomposite showed deficient apatite nucleation on its surface, forming a non-continuous layer (Figure 5a). This non-monotonous dependence of the bioactivity is again a reflection of the different topology of the silica phase in the composites. Above silica percolation concentrations ($\geq$25 wt% of silica), the continuous silica network has less free silanols on its boundary surface, and thus the HAp nuclei can only grow from the pre-existing nucleating sites of polymer matrix. Besides, a dense and continuous silica network can completely hinder the swelling of the organic polymer matrix in the aqueous medium and impedes the diffusion of SBF ions into the polymer matrix, leading to a lesser dissolution of the silica network at the surface, which explains the decreased HAp deposition on the 30% silica samples.

No significant differences among nanocomposites with different silica contents were detected in the direct MTS assay with seeded MC3T3 pre-osteoblastic cells (Figure 6). Nevertheless, the number of viable cells is significantly higher in the nanocomposites after 7 and 21 days of culture compared to the copolymer samples. In addition, all samples except the control, polystyrene coverslips, show a significant cellular growth with the culture time suggesting an adequate cellular proliferation.

The results of the immunocytochemistry assays (Figure 7) suggest that the materials provide an adequate environment for osteoblastic differentiation and specific ECM production, in spite of the fact that neither mineralization-induction medium nor any supplements for bone-differentiation were used during the cultures. Nanocomposites with 15% and 30% of silica showed better results than the neat copolymer and the 5% silica nanocomposite; this shows that silica content, and maybe the higher stiffness of the surface of the material, is favourable for osteoblast behaviour.[39,40] Osteoblastic differentiation is sensitive to substrate chemistry, being neutral hydrophilic (OH−) and positively charged (NH_2−)

patterns more advantageous than negatively charged (COOH−) and hydrophobic (CH_3−), up-regulating osteoblast-specific gene expression, enzymatic activity of alkaline phosphatase, and ECM mineralization.[41] Besides, as it was found in Khatiwala et al.,[42] substrate stiffness can influence MC3T3-E1 behaviour: migration speed (affected by filopodia formation, elongation and in general mobility), proliferation rate and matrix mineralization increase due to better cytoskeleton development and focal adhesions on rigid surfaces. A further support for osteoblastic differentiation and specific ECM production was given by the results of von Kossa staining (Figure 8), which confirm the beginning of calcium deposition and matrix mineralization process at 14 days of culture and its progress for 21 days of culture. The extent of ECM mineralization is an indicator of a mature osteoblast phenotype; images reveal it to be greater on the nanocomposites than on the copolymer, showing a mechanical and chemical effect on the mineralization process due to silica.

Conclusions

Poly(CLMA-co-HEA)/silica nanocomposites are stable, optically transparent and uniform, and the silica network is finely interpenetrated with copolymer matrix. The silica phase improves the mechanical properties of the organic copolymer matrix; the constraining effect of the extended dense silica network restricts the copolymer chains mobility and leads to the significant reinforcement of the nanocomposites around the percolation threshold. The storage modulus, the glass transition temperature and the width of the transition show an increase with the silica content, whereas the heat capacity jump at the glass transition and the equilibrium water content decrease, reflecting the reinforcing effect on the organic matrix provided by the build-up of the silica network and its percolation above the threshold of approximately 15 wt% silica content. HAp crystals nucleate and grow on the surface of these biomaterials, and this bioactivity seems to be greatest at intermediate silica mass percentages (15 wt% silica), as a consequence of the topological features of the silica phase in the nanocomposite. The materials are non-cytotoxic and promote the osteoblastic differentiation and the beginning of the osteogenic process of MC3T3 cells *in vitro*. The presence of the silica phase greatly increases the cell proliferation and differentiation rates compared to those of the neat copolymer and positive control.

Declaration of conflicting interests

The authors declared no potential conflicts of interest with respect to the research, authorship, and/or publication of this article.

Funding

The authors acknowledge the financial support from the Spanish Ministry of Science and Innovation through projects DPI2010-20399-c04-03 and MAT2011-28791-C03-02. AJCF acknowledges support through Torres Quevedo grant PTQ08-02-06321. GGF and MMP acknowledge support of CIBER-BBN initiative, financed by Instituto de Salud Carlos III (Spain) with the assistance of the European Regional Development Fund.

References

1. Ivirico JL, Martinez EC, Sanchez MS, et al. Structure and properties of methacrylate-endcapped caprolactone networks with modulated water uptake for biomedical applications. *J Biomed Mater Res Part B, Appl Biomater* 2007; 83: 266–275.
2. Ivirico JLE, Salmerón-Sánchez M, Ribelles JLG, et al. Proliferation and differentiation of goat bone marrow stromal cells in 3D scaffolds with tunable hydrophilicity. *J Biomed Mater Res Part B: Appl Biomater* 2009; 91B: 277–286.
3. Escobar Ivirico JL, Salmerón Sánchez M, Sabater i Serra R, et al. Structure and properties of poly(ε-caprolactone) networks with modulated water uptake. *Macromol Chem Phys* 2006; 207: 2195–2205.
4. Boxberg Y, Schnabelrauch M, Vogt S, et al. Effect of hydrophilicity on the properties of a degradable polylactide. *J Polym Sci Part B: Polymer Phys* 2006; 44: 656–664.
5. Olmedilla MP, Lebourg M, Ivirico JLE, et al. In vitro 3D culture of human chondrocytes using modified ε-caprolactone scaffolds with varying hydrophilicity and porosity. *J Biomater Appl* 2012; 27: 299–309.
6. Salgado AJ, Coutinho OP and Reis RL. Bone tissue engineering: state of the art and future trends. *Macromol Biosci* 2004; 4: 743–765.
7. Sprio S, Ruffini A, Valentini F, et al. Biomimesis and biomorphic transformations: new concepts applied to bone regeneration. *J Biotechnol* 2010; 156: 347–355.
8. Barone DTJ, Raquez JM and Dubois P. Bone-guided regeneration: from inert biomaterials to bioactive polymer (nano) composites. *Polym Adv Technol* 2011; 22: 463–475.
9. Jones JR. New trends in bioactive scaffolds: The importance of nanostructure. *J Eur Ceramic Soc* 2009; 29: 1275–1281.
10. Paital SR and Dahotre NB. Calcium phosphate coatings for bio-implant applications: Materials, performance factors, and methodologies. *Mater Sci Eng: R: Reports* 2009; 66: 1–70.
11. Arcos D and Vallet-Regi M. Sol-gel silica-based biomaterials and bone tissue regeneration. *Acta Biomater* 2010; 6: 2874–2888.
12. Boccaccini AR, Erol M, Stark WJ, et al. Polymer/bioactive glass nanocomposites for biomedical applications: A review. *Compos Sci Technol* 2010; 70: 1764–1776.
13. Hanemann T and Szabó DV. Polymer-nanoparticle composites: from synthesis to modern applications. *Materials* 2010; 3: 3468–3517.

14. Pantaleón R and González-Benito J. Structure and thermostability of PMMA in PMMA/silica nanocomposites: Effect of high-energy ball milling and the amount of the nanofiller. *Polymer Compos* 2010; 31: 1585–1592.
15. Bera O, Pilić B, Pavličević J, et al. Preparation and thermal properties of polystyrene/silica nanocomposites. *Thermochim Acta* 2011; 515: 1–5.
16. Yan S, Yin J, Cui L, et al. Apatite-forming ability of bioactive poly(l-lactic acid)/grafted silica nanocomposites in simulated body fluid. *Colloid Surfac B, Biointerf* 2011; 86: 218–224.
17. Zhang ZG, Li ZH, Mao XZ, et al. Advances in bone repair with nanobiomaterials: mini-review. *Cytotechnology* 2011; 63: 437–443.
18. Salinas AJ, Esbrit P and Vallet-Regi M. A tissue engineering approach based on the use of bioceramics for bone repair. *Biomater Sci* 2013; 1: 40–51.
19. Izquierdo-Barba I, Salinas AJ and Vallet-Regí M. Bioactive glasses: From macro to nano. *International Journal of Applied Glass Science* 2013; 4: 149–161.
20. Hajji P, David L, Gerard JF, et al. Synthesis, structure, and morphology of polymer–silica hybrid nanocomposites based on hydroxyethyl methacrylate. *J Polym Sci Part B: Polym Phys* 1999; 37: 3172–3187.
21. Catauro M, Raucci MG, De Gaetano F, et al. Sol-gel synthesis, characterization and bioactivity of polycaprolactone/SiO_2 hybrid material. *J Mater Sci* 2003; 38: 3097–3102.
22. Catauro M, Raucci MG, de Gaetano F, et al. Sol–gel synthesis, structure and bioactivity of Polycaprolactone/CaO • SiO_2 hybrid material. *J Mater Sci: Mater Med* 2004; 15: 991–995.
23. Nie K, Pang W, Wang Y, et al. Effects of specific bonding interactions in poly(ε-caprolactone)/silica hybrid materials on optical transparency and melting behavior. *Mater Lett* 2005; 59: 1325–1328.
24. Zou H, Wu S and Shen J. Polymer/silica nanocomposites: Preparation, characterization, properties, and applications. *Chemical Reviews* 2008; 108: 3893–3957.
25. Poologasundarampillai G, Ionescu C, Tsigkou O, et al. Synthesis of bioactive class II poly(γ-glutamic acid)/silica hybrids for bone regeneration. *J Mater Chem* 2010; 20: 8952.
26. Lee E-J, Teng S-H, Jang T-S, et al. Nanostructured poly(ε-caprolactone)–silica xerogel fibrous membrane for guided bone regeneration. *Acta Biomater* 2010; 6: 3557–3565.
27. Vallés Lluch A, Gallego Ferrer G and Monleón Pradas M. Biomimetic apatite coating on P(EMA-co-HEA)/SiO_2 hybrid nanocomposites. *Polymer* 2009; 50: 2874–2884.
28. Kawai T, Ohtsuki C, Kamitakahara M, et al. In vitro apatite formation on polyamide containing carboxyl groups modified with silanol groups. *J Mater Sci: Mater Med* 2007; 18: 1037–1042.
29. Oliveira AL, Malafaya PB and Reis RL. Sodium silicate gel as a precursor for the *in vitro* nucleation and growth of a bone-like apatite coating in compact and porous polymeric structures. *Biomaterials* 2003; 24: 2575–2584.
30. Rhee SH. Effect of silica content on the bioactivity and mechanical properties of poly(ε-caprolactone)/silica hybrid containing calcium salt. *Key Eng Mater* 2003; 240–242: 187–190.
31. Kokubo T. Design of bioactive bone substitutes based on biomineralization process. *Mater Sci Eng: C* 2005; 25: 97–104.
32. Rimer JD, Trofymluk O, Navrotsky A, et al. Kinetic and thermodynamic studies of silica nanoparticle dissolution. *Chem Mater* 2007; 19: 4189–4197.
33. Hernández JCR, Pradas MM and Ribelles JLG. Properties of poly(2-hydroxyethyl acrylate)-silica nanocomposites obtained by the sol–gel process. *J Non-Crystalline Solid* 2008; 354: 1900–1908.
34. Vallés-Lluch A, Costa E, Gallego Ferrer G, et al. Structure and biological response of polymer/silica nanocomposites prepared by sol–gel technique. *Compos Sci Technol* 2010; 70: 1789–1795.
35. Vallés-Lluch A, Rodríguez-Hernández JC, Ferrer GG, et al. Synthesis and characterization of poly(EMA-co-HEA)/SiO_2 nanohybrids. *Eur Polym J* 2010; 46: 1446–1455.
36. Vallés-Lluch A, Ferrer GG and Pradas MM. Effect of the silica content on the physico-chemical and relaxation properties of hybrid polymer/silica nanocomposites of P(EMA-co-HEA). *Eur Polym J* 2010; 46: 910–917.
37. Kokubo T and Takadama H. How useful is SBF in predicting in vivo bone bioactivity? *Biomaterials* 2006; 27: 2907–2915.
38. Brinker CJ, Keefer KD, Schaefer DW, et al. Sol-gel transition in simple silicates. *J Non-crystalline Solid* 1982; 48: 47–64.
39. Bigerelle M, Ponche A and Anselme K. Relative influence of surface topography and surface chemistry on cell response to bone implant materials. Part 2: biological aspects. *Proc Institut Mech Eng, Part H: J Eng Med* 2010; 224: 1487–1507.
40. Palacio ML and Bhushan B. Bioadhesion: A review of concepts and applications. *Philos Transact Ser A, Math, Phys, Eng Sci* 2012; 370: 2321–2347.
41. Keselowsky BG, Collard DM and Garcia AJ. Integrin binding specificity regulates biomaterial surface chemistry effects on cell differentiation. *Proc Natl Acad Sci USA* 2005; 102: 5953–5957.
42. Khatiwala CB, Peyton SR and Putnam AJ. Intrinsic mechanical properties of the extracellular matrix affect the behavior of pre-osteoblastic MC3T3-E1 cells. *Am J Physiol – Cell Physiol* 2006; 290: C1640–C1650.